Rapid Communications

Landau levels, Bardeen polynomials, and Fermi arcs in Weyl semimetals: Lattice-based approach to the chiral anomaly

Jan Behrends,[1] Sthitadhi Roy,[2,3,1] Michael H. Kolodrubetz,[4,5,6] Jens H. Bardarson,[7,1] and Adolfo G. Grushin[4,8]

[1]*Max-Planck-Institut für Physik komplexer Systeme, D-01187 Dresden, Germany*

[2]*Physical and Theoretical Chemistry, Oxford University, South Parks Road, Oxford OX1 3QZ, United Kingdom*

[3]*Rudolf Peierls Centre For Theoretical Physics, Clarendon Laboratory, Oxford University, Parks Road, Oxford OX1 3PU, United Kingdom*

[4]*Department of Physics, University of California, Berkeley, California 94720, USA*

[5]*Materials Sciences Division, Lawrence Berkeley National Laboratory, Berkeley, California 94720, USA*

[6]*Department of Physics, The University of Texas at Dallas, Richardson, Texas 75080, USA*

[7]*Department of Physics, KTH Royal Institute of Technology, SE-106 91 Stockholm, Sweden*

[8]*Institut Néel, CNRS and Université Grenoble Alpes, F-38042 Grenoble, France*

(Received 25 July 2018; revised manuscript received 30 January 2019; published 1 April 2019)

Condensed matter systems realizing Weyl fermions exhibit striking phenomenology derived from their topologically protected surface states as well as chiral anomalies induced by electromagnetic fields. More recently, inhomogeneous strain or magnetization were predicted to result in chiral electric $\mathbf{E}_5$ and magnetic $\mathbf{B}_5$ fields, which modify and enrich the chiral anomaly with additional terms. In this Rapid Communication, we develop a lattice-based approach to describe the chiral anomaly, which involves Landau and pseudo-Landau levels and treats all anomalous terms on equal footing, while naturally incorporating Fermi arcs. We exemplify its potential by physically interpreting the largely overlooked role of Fermi arcs in the covariant (Fermi level) contribution to the anomaly and revisiting the factor of $1/3$ difference between the covariant and consistent (complete band) contributions to the $\mathbf{E}_5 \cdot \mathbf{B}_5$ term in the anomaly. Our framework provides a versatile tool for the analysis of anomalies in realistic lattice models as well as a source of simple physical intuition for understanding strained and magnetized inhomogeneous Weyl semimetals.

DOI: 10.1103/PhysRevB.99.140201

Quantum anomalies describe the breaking of a classical symmetry by quantum fluctuations [1]. The chiral anomaly, the nonconservation of the chiral charge of three-dimensional Weyl fermions, is relevant to different domains in physics since Weyl fermions mediate the pion decay into photons [2,3] and are emergent quasiparticles in Weyl semimetals [4–9]. The physics is particularly transparent in the Landau level picture pioneered by Nielsen and Ninomiya [10], requiring only basic quantum mechanics. In a magnetic field $\mathbf{B}$, the conical Weyl dispersion evolves into Landau levels with a degeneracy proportional to $|\mathbf{B}|$ [10]. Since momentum along the direction of the magnetic field remains a good quantum number, the Landau levels disperse in that direction, with the zeroth Landau level having a linear dispersion with a sign determined by the chirality; all other Landau levels have a quadratic dispersion. The zeroth Landau levels of the left- and right-handed Weyl fermions furthermore connect at high energy. Consequently, an electric field ($\mathbf{E}$) with a component along the dispersion transfers left-handed fermions to right-handed fermions (or vice versa), resulting in a nonconservation of left and right particle numbers proportional to $\mathbf{E} \cdot \mathbf{B}$ [1,10,11].

Other fields, such as chiral pseudoelectromagnetic fields, torsion, or curvature, activate the chiral anomaly beyond $\mathbf{E}$ and $\mathbf{B}$ [12–22]. Weyl semimetals are ideal to probe the chiral anomaly in the presence of chiral pseudoelectromagnetic fields. To motivate this, recall that their low-energy degrees of freedom are pairs of chiral Weyl quasiparticles at topologically protected band touchings (Weyl nodes), separated in energy-momentum space by a four-vector b_μ [9]. A space- and time-dependent b_μ, as in strained or inhomogeneously magnetized Weyl semimetals [15] or ^{3}He [23,24], generates chiral pseudomagnetic ($\mathbf{B}_5 = \nabla \times \mathbf{b}$) and pseudoelectric ($\mathbf{E}_5 = -\partial_t \mathbf{b} - \nabla b_0$) fields, which couple with opposite signs to opposite chiralities [16,17,25–28]. These pseudofields enhance or generalize phenomena ranging from transport to interface physics [16,17,29–39]. Unlike $\mathbf{B}$, which generates Landau levels dispersing in opposite directions for opposite chiralities, $\mathbf{B}_5$ generates pseudo-Landau levels that disperse in the *same* direction for both chiralities [16,17,25,26,40].

Applying the Landau level picture to chiral fields leads to puzzling conclusions: For example, because of the chirality-independent dispersion of the zeroth pseudo-Landau level due to $\mathbf{B}_5$, $\mathbf{E}$ increases (or decreases) the number of fermions for *both* chiralities at a rate proportional to $\mathbf{E} \cdot \mathbf{B}_5$, giving an apparent nonconservation of the total charge. This is expressed as the so-called *covariant* anomaly [1,40]

$$\partial_\mu J^\mu_{5,\mathrm{cov}} = \frac{1}{2\pi^2}(\mathbf{E} \cdot \mathbf{B} + \mathbf{E}_5 \cdot \mathbf{B}_5), \tag{1}$$

$$\partial_\mu J^\mu_{\mathrm{cov}} = \frac{1}{2\pi^2}(\mathbf{E}_5 \cdot \mathbf{B} + \mathbf{B}_5 \cdot \mathbf{E}). \tag{2}$$

Neither the covariant chiral ($J^\mu_{5,\mathrm{cov}} = J^\mu_{L,\mathrm{cov}} - J^\mu_{R,\mathrm{cov}}$) nor vector ($J^\mu_{\mathrm{cov}} = J^\mu_{L,\mathrm{cov}} + J^\mu_{R,\mathrm{cov}}$) currents are conserved. In field

theory, to explicitly restore charge conservation, the covariant currents are supplemented by Bardeen polynomials δj^μ, which act as boundary conditions for the accumulated charge at the cutoff energy [41–44]. This procedure defines the *consistent* anomaly [1,40]

$$\partial_\mu J_5^\mu = \frac{1}{2\pi^2}\left(\mathbf{E}\cdot\mathbf{B} + \frac{1}{3}\mathbf{E}_5\cdot\mathbf{B}_5\right), \tag{3}$$

$$\partial_\mu J^\mu = 0. \tag{4}$$

The consistent anomaly conserves charge, and thus determines observables [42,45] by discarding unphysical responses [40–42,46]. The Bardeen polynomials, however, sacrifice intuition of the covariant picture based on Landau levels and obfuscate the restoration of charge conservation in specific lattice implementations.

Despite the field theory of the consistent and covariant anomalies being well understood for a long time [40], a simple physical picture of their origin on a lattice, with guaranteed charge conservation, is still missing. In this Rapid Communication, we provide such a picture using as building blocks the Landau and pseudo-Landau levels. It leads to our two main results: First, we identify the Fermi arcs as a source for the covariant anomaly terms of Eq. (2) and relate them to the Bardeen polynomials. Second, we show that when $\mathbf{B}_5 > \mathbf{B}$, the Fermi surface twists into a bowtie shape, a property central to our understanding of how the term $\mathbf{E}\cdot\mathbf{B}_5$ redistributes charge within the sample. Our picture allows us to address as well the 1/3 disparity between the second term in Eq. (3) and Eq. (1). We argue that a necessary condition for its identification is a $\mathbf{B}_5$ profile that spatially separates chiral charge creation and annihilation. Similar to how Landau levels simplified our understanding of the chiral anomaly [10], we use pseudo-Landau levels (developed in Ref. [17]) to provide a unified and simple lattice picture of the consistent and covariant anomalies with specific implications for experiment.

Our starting point is the Weyl semimetal model [46]

$$\mathcal{H} = v[\sin(k_y)\sigma_x - \sin(k_x)\sigma_y]\tau_z + v\sin(k_z)\tau_y + m\tau_x + t\sum_i[1-\cos(k_i)]\tau_x + v\sum_\mu u^\mu b_\mu, \tag{5}$$

with $a = 1$ the lattice constant, σ_i (τ_i) spin (orbital) Pauli matrices, and $u^\mu = (\sigma_z\tau_y, -\sigma_x\tau_x, -\sigma_y\tau_x, \sigma_z)$. For small $b_\mu = (b_0, \mathbf{b})$ and $m^2 < v^2|\mathbf{b}^2 - b_0^2|$, the model has one pair of Weyl nodes near Γ [46,47]. Unless stated otherwise, we set $m = 0$ and $t = 2v/\sqrt{3}$. When $\mathbf{b}$ is oriented along a reciprocal lattice vector, this parameter choice gives two Weyl nodes located at $\pm\mathbf{b}[1 + O(b_0^2)] + O(b_j^5)$ and energies $\pm v b_0[1 + O(b_j^2)] + O(b_0^3)$. Our results also apply to generalizations of Eq. (5) that model Dirac (e.g., Cd_3As_2, Na_3Bi) and Weyl (e.g., TaAs family) materials [48–50]. We further define $\gamma^\mu = (\tau_x, i\sigma_y\tau_y, -i\sigma_x\tau_y, i\tau_z)$ and $\gamma^5 = i\gamma^0\gamma^1\gamma^2\gamma^3 = \sigma_z\tau_y$, such that $u^\mu = \gamma^0\gamma^\mu\gamma^5$ and the space-dependent chiral charge density is

$$J_5^0(\mathbf{x}) \equiv \rho_5(\mathbf{x}) = \sum_{n\in\text{occ.}}\langle\psi_n(\mathbf{x})|\gamma^5|\psi_n(\mathbf{x})\rangle. \tag{6}$$

The charge density $\rho(\mathbf{x})$ is obtained by replacing γ^5 with the identity in Eq. (6). While our lattice model (5) includes a τ_x term that explicitly breaks conservation of ρ_5, we show in Ref. [51] how this effect is controlled.

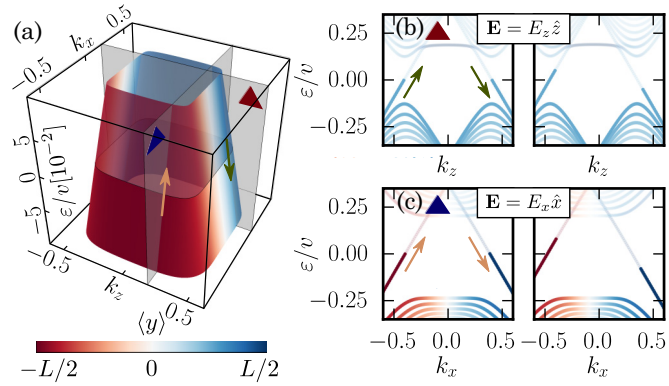

FIG. 1. Anomalies due to $\mathbf{E}\cdot\mathbf{B}$ and $\mathbf{E}\cdot\mathbf{B}_5$. (a) The spectrum of Hamiltonian (5) for a slab finite along y, showing the coexisting Fermi arcs and Landau levels of $\mathbf{B} = B\hat{z}$. The color scale denotes the wave function's position along y. (b), (c) The Landau (pseudo-Landau) levels of $\mathbf{B}$ ($\mathbf{B}_5$) on the red (blue) triangle plane show the anomaly in the presence of $\mathbf{E} = E_z\hat{z}$ ($\mathbf{E} = E_x\hat{x}$), where the spectral flow at the Fermi surface is shown by green (orange) arrows. We implement $\mathbf{E}$ using the gauge choice $\mathbf{k} \to \mathbf{k} - \mathbf{E}t$. The left panels show the occupation at $t = 0$, while the right panels show the dispersion for $t > 0$ with $E_{x,z}t = 0.08$ and the same momenta occupied as in the left panels [51]. Here, $L = 100$ and $\ell_B = 1/\sqrt{B} = 11.2$.

The Hamiltonian (5) (with $v = 1$) derives from an effective field theory with action

$$\mathcal{S} = \int d^4x\,\bar{\psi}[\gamma^\mu(i\partial_\mu - A_\mu - b_\mu\gamma^5) - m]\psi, \tag{7}$$

where $\bar{\psi} = \psi^\dagger\gamma^0$ and repeated indices are summed. $\mathcal{S}$ yields two species of Weyl fermions of opposite chiralities, coupled to an external chiral field b_μ and a vector field A_μ, and separated by b_μ for $m = 0$. The lattice regularization is given by the Wilson map $k_i \to \sin k_i$ [52], and $m \to m + t\sum_i(1 - \cos k_i)$ [53].

Spatial and temporal variations of $\mathbf{b}$ generate the chiral fields $\mathbf{B}_5 = \nabla\times\mathbf{b}$ and $\mathbf{E}_5 = -\partial_0\mathbf{b}$. The simplest realization of $\mathbf{B}_5$ occurs at the boundary of any Weyl semimetal with vacuum, where the Weyl node separation b_μ goes to zero [17,26,40]. For example, for a slab along y, $\mathbf{b}(y) = b_z[\Theta(y - L/2) - \Theta(y + L/2)]\hat{z}$ gives $\mathbf{B}_5(y) = b_z[\delta(y - L/2) - \delta(y + L/2)]\hat{x}$, localized at the surface, which generates surface pseudo-Landau levels dispersing along $\pm k_x$, with opposite signs at each surface [17]. Their Fermi surface traces an arc, establishing the correspondence between surface pseudo-Landau levels induced by $\mathbf{B}_5$ and topological surface states. Analogously, a uniform external magnetic field $\mathbf{B} = B\hat{z}$ parallel to the Weyl node separation leads to a spectrum hosting bulk Landau levels dispersing along $\pm k_z$, where the sign is set by the Weyl node chirality. When both $\mathbf{B}$ and a surface $\mathbf{B}_5$ are present, Landau and pseudo-Landau levels coexist and the Fermi surface at the Fermi energy ε_F (set to $\varepsilon_F = 0$ hereafter) traces a rectangle [54]; see Fig. 1(a) [55,56].

The coexistence of Landau and pseudo-Landau levels provides an ideal platform to discuss the anomalies. Applying $\mathbf{E} = E_z\hat{z}$ pumps charges of one chirality to the other,

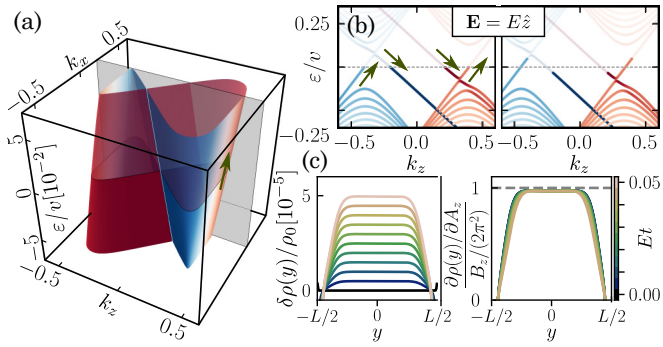

FIG. 2. Anomaly due to $\mathbf{E}\cdot\mathbf{B}_5$ with a constant bulk $\mathbf{B}_5 = B_5\hat{z}$. (a) Energy spectrum with the same color coding and boundary conditions as Fig. 1. (b) The pseudo-Landau levels of $\mathbf{B}_5$ show an anomaly when $\mathbf{E} = E\hat{z}$ with the spectral flow indicated by the green arrows. The left panel shows the occupation at $k_x = 0.2$ [gray plane in (a)] at $t = 0$; in the right panel, $Et = 0.05$. (c) Left: The spatial profile of the charge $\delta\rho$ relative to that at $t = 0$, normalized by the total charge ρ_0 for different times (colors), showing a surface to bulk charge redistribution. The y axis is chosen such that only the (positive) bulk contribution is visible, which is exactly canceled by the (negative) surface contribution. Right: Derivative of the density with respect to the vector potential A for different times, which equals $\partial_{A_z}\rho = B_5/(2\pi^2)$ in the bulk (dashed line). The derivatives with respect to vector potential and time are related via $\partial_t\rho = -\mathbf{E}\cdot\partial_{\mathbf{A}}\rho$. In (a) and (b), $L = 100$ and $\ell_5 = 1/\sqrt{B_5} = 11.1$; in (c), $L = 200$ and $\ell_5 = 15.8$.

connecting Landau levels of $\mathbf{B}$ through the band bottom and realizing the $\mathbf{E}\cdot\mathbf{B}$ term in Eq. (3) [10] [see Fig. 1(b)]. Similarly, since the pseudo-Landau levels disperse along $\pm k_x$ on each surface, applying $\mathbf{E} = E_x\hat{x}$ depletes charges from one surface and generate charges on the other [Fig. 1(c)]. We can interpret [10] this as an anomaly of *each* surface state due to $\mathbf{E}\cdot\mathbf{B}_5$. In contrast to the chiral anomaly in the absence of chiral fields, where the total charge is locally conserved, the spatial separation of the two surfaces leads to an apparent violation of local charge conservation, as in Eq. (2). Our pseudo-Landau level picture demonstrates the surface origin of the covariant anomaly, $\sim\mathbf{E}\cdot\mathbf{B}_5$.

Our picture tracks how charge is explicitly conserved. The spectral flow between the pseudo-Landau levels at each surface happens via the bulk Landau levels connecting them, fixing local charge conservation. The effect of $\mathbf{E}$ results in an adiabatic shift of k_x, which via position-momentum locking [17] generates a Hall current

$$\delta\mathbf{j} = -\frac{1}{2\pi^2}b_z E_x\hat{y}. \tag{8}$$

We can interpret this as the net current flowing along $\hat{y}$ between surfaces through the bottom of the band. In the bulk, b_z is constant leading to $\nabla\cdot\delta\mathbf{j} = 0$ and no accumulation of charge. At the surface, the Weyl node separation varies, leading to a finite divergence of the spatial current, positive on one surface and negative on the other.

Similarly, more general profiles of $\mathbf{B}$ and $\mathbf{B}_5$ can be understood in terms of Landau and pseudo-Landau levels. For instance, a uniform bulk $\mathbf{B}_5 \parallel \hat{z}$ arises from $\mathbf{b} = B_5 y\hat{x}$. Its spectrum [Fig. 2(a)] shows a characteristic butterfly Fermi surface, obtained from the rectangular Fermi surface [Fig. 1(a)] by noticing that the two bulk Landau levels have lengths $\mathbf{B}\pm\mathbf{B}_5$. When $\mathbf{B}_5 > \mathbf{B}$, the Fermi surface twists, leading to Fig. 2(a) (found to lead to peculiar quantum oscillation signals in an unrelated context [57]). An $\mathbf{E} = E\hat{z}$ parallel to $\mathbf{B}_5$ [Figs. 2(b) and 2(c)] makes the bulk gain charge above the Fermi level (upward arrows), while the surface loses charge (downward arrows). This is consistent with the lattice numerics [Fig. 2(e)] where the spatial profile of the charge relative to that at $t = 0$ is shown for different times.

Our previous examples (Figs. 1 and 2) are a consequence of the covariant anomaly which only considers the depletion and growth of charges at the Fermi level. By construction, the corresponding current $J^\mu_{\rm cov}$ misses information from states away from the Fermi level, and thus it is not conserved as dictated by Eq. (2) [51]. The consistent current J^μ is obtained from the covariant current by adding the Bardeen polynomials δj^μ such that $\partial_\mu(J^\mu_{\rm cov} + \delta j^\mu) = \partial_\mu J^\mu = 0$ [41,42]. Using Eq. (2) and the definition of the pseudofields,

$$\delta j^0 = \frac{1}{2\pi^2}\mathbf{b}\cdot\mathbf{B}, \quad \delta\mathbf{j} = \frac{1}{2\pi^2}(b_0\mathbf{B} - \mathbf{b}\times\mathbf{E}). \tag{9}$$

Comparing (9) to (8) of our first example (Fig. 1), we identify the latter as a part of the Bardeen polynomials [40]. The benefit of the Landau level approach is its intuitive interpretation: In the first example, $\mathbf{E}_5 = \mathbf{0}$ and the finite $\mathbf{E}\cdot\mathbf{B}_5$ pumps charge from one surface to another via the anomalous Hall effect [Eq. (8)] through $\partial_t J^0_{\rm cov} = \mathbf{E}\cdot\mathbf{B}_5/(2\pi^2)$. Our second example, Fig. 2, can be interpreted similarly. In the bulk charge grows as $\partial_t J^0_{\rm cov} = \mathbf{E}\cdot\mathbf{B}_5/(2\pi^2)$ locally while at the surface, charge is depleted since $\mathbf{B}_5$ has the opposite sign. The corresponding current (9) pumps charge from the surface to the bulk. Since $\mathbf{b} = B_5 y\hat{x}$, there are local currents in the bulk $\delta\mathbf{j} \sim B_5 E y\hat{y}$ and $\nabla\cdot\delta\mathbf{j} = \mathbf{B}_5\cdot\mathbf{E}/(2\pi^2)$ is precisely the growth rate of local charge [Fig. 2(c)], reconciling the Fermi surface (covariant) picture with the charge conserving (consistent) picture on the lattice [58].

Moving on to spatiotemporally varying Weyl node separations, consider first $\mathbf{b} = -E_5 t\hat{z}$, yielding uniform $\mathbf{E}_5 \parallel \hat{z}$. A $\mathbf{B} \neq \mathbf{0}$ activates the second term of (2), suggesting that charge is created at the Fermi surface at a rate $\mathbf{E}_5\cdot\mathbf{B}/(2\pi^2)$. For our lattice model (5), $\mathbf{E}_5$ shifts the band bottom, pushing charge above a fixed energy [Fig. 3(a)]. Rigid shifts of the band conserve total charge, giving the consistent picture of the anomaly. However, if one insists on only considering the low-energy gray region in Fig. 3(a), the charge appears to emerge from the vacuum, as expected from the covariant anomaly. The connection between these pictures is shown in Fig. 3(b), where charge growth near the Fermi surface equals charge loss near the band bottom, which in turn equals the Bardeen polynomial δj^0, Eq. (9).

We end by addressing the factor of $1/3$ disparity between the prefactors of the $\mathbf{E}_5\cdot\mathbf{B}_5$ anomalies. This difference implies that the band bottom current must add $-2/3$ to the Fermi surface contribution, irrespective of the precise pseudofield profile. One may argue that this factor arises from the topological nature of the Bardeen polynomials [44], yet we find that topology alone does not explain the conditions which give $1/3$ for a generic lattice model.

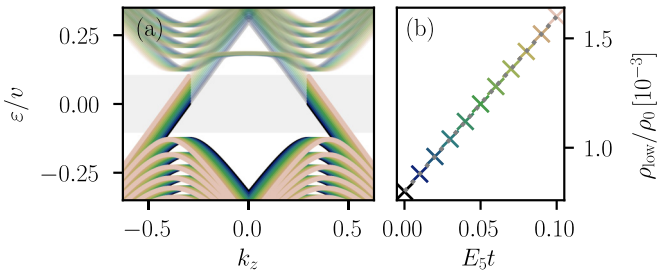

FIG. 3. Anomaly due to $\mathbf{E}_5 \cdot \mathbf{B}$. (a) Occupation at $k_x = 0.2$ and $\mathbf{B} \parallel \mathbf{E}_5 \parallel \hat{z}$ for different times [different colors, (b)], where dark (light) colors represent filled (empty) states and the gray shaded region is the low-energy regime, isolating the covariant anomaly. We implement $\mathbf{E}_5$ by $\mathbf{b} \to \mathbf{b} - \mathbf{E}_5 t$ and use the same boundary conditions as Fig. 1 with $L = 100$ lattice sites and $\ell_B = 11.2$. (b) The charge in the gray low-energy regime $\rho_{\rm low}$ linearly increases with $E_5 t$. Since the total charge is conserved, the charge in the band bottom decreases at the same rate (not shown).

To illustrate the conditions for isolating the 1/3, consider [36]

$$\mathbf{b} = \frac{c_B}{2}\left[\mathrm{erf}\left(\frac{y-\frac{L}{4}}{\sqrt{2}\xi}\right) - \mathrm{erf}\left(\frac{y+\frac{L}{4}}{\sqrt{2}\xi}\right) - 1\right]\hat{x} + b_z\hat{z}, \quad (10)$$

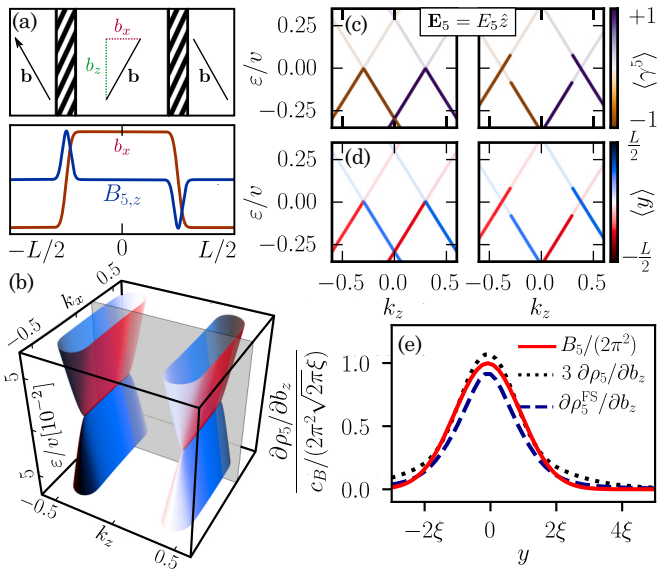

FIG. 4. Anomaly due to $\mathbf{E}_5 \cdot \mathbf{B}_5$. (a) The Weyl node separation (10) and its corresponding $\mathbf{B}_5$. (b) Energy spectrum with a real space color encoding that reflects the periodic boundary conditions. (c), (d) Where $\mathbf{B}_5 > \mathbf{0}$ [red in (d)], a parallel $\mathbf{E}_5$ pushes left- and right-handed chiral charges above and below the Fermi level, respectively, annihilating chiral charge. Where $\mathbf{B}_5 < \mathbf{0}$ (blue), chiral charge is created. (e) The spatial distribution of chiral charge creation and annihilation follows and equals $\mathbf{B}_5$ (red solid line) for charges $\rho_5^{\rm FS}$ traversing the original Fermi surface (blue dashed line). With all bands, the total chiral charge creation is ∼1/3 of that at the Fermi surface, as predicted by the consistent anomaly (black dotted line). We use $L = 360$, a $\mathbf{B}_5$ broadening $\xi = 6$ and peak height $c_B = 1.25$, and a delta function broadening $\eta = 10^{-6}v$ [51].

with c_B a constant and $\mathrm{erf}(x)$ the error function [Fig. 4(a)]. In a periodic system of length L in the y direction, this profile realizes interfaces at $\pm L/4$ between two Weyl semimetals with different node separations, connected by regions where $\mathbf{b}$ smoothly changes to give $\mathbf{B}_5 = B_5(y)\hat{z}$ with $B_5(y) = \frac{c_B}{\sqrt{2\pi}\xi}[e^{-(y-\frac{L}{4})^2/(2\xi^2)} - e^{-(y+\frac{L}{4})^2/(2\xi^2)}]$. This profile maintains the useful property that the two chiralities (eigenstates of γ^5) are well separated in momentum space [Fig. 4(c)]. Adding $\mathbf{E}_5 \parallel \mathbf{B}_5$ to produce a chiral anomaly, chiral charge (6) is created/annihilated in spatially separated regions [Fig. 4(d)], at a rate that closely follows the spatial profile of $\mathbf{B}_5$ as expected from Eq. (3) [Fig. 4(e)]. The Fermi surface contribution to the chiral charge is calculated as

$$\frac{d\rho_5^{FS}(y)}{d\mathbf{b}} = \sum_n \langle\psi_n|\gamma^5\Pi_y|\psi_n\rangle\langle\psi_n|\partial_{\mathbf{b}}\mathcal{H}|\psi_n\rangle\delta(\mu - \varepsilon_n), \quad (11)$$

with Π_y the projector to the position y [51]. Comparing the chiral charge pumped at the Fermi surface and that in the full spectrum to the expected value proportional to B_5, we see that they are close, but neither perfectly reproduces the field theory prediction.

To determine the factors behind this mismatch we note that the erf profile minimizes the spatial overlap between regions of chiral charge creation and annihilation ($\partial\rho_5/\partial b_z > 0$ and < 0 at $y \approx +L/4$ and $y \approx -L/4$, respectively). However, for both chiralities, there exist regions in momentum space [light/dark regions in Fig. 4(b)] where the states are not well localized in real space. These regions spread out with increasing ξ, such that the erf profile evolves into a sinusoidlike function, resulting in a poorer match between the $B_5(y)$ profile and the chiral charge response [51]. The sensitivity of the result to these regions, highlighted by the failure of the sinusoidlike profile where no clear spatial separation exists, implies that the value 1/3 is modified by such effects for generic profiles of $\mathbf{B}_5$. This detrimental overlap is minimized if $L \gg \xi \gg a$ is satisfied, allowing the intriguing possibility that an exact 1/3 may be recovered in this limit. Finally, all anomaly terms present finite size and quadratic corrections to the low-energy field theory (7), which we discuss in Ref. [51].

In summary, we have provided an intuitive lattice picture that is based on Landau and pseudo-Landau levels and connects the covariant and consistent anomalies. We explicitly identified the Hall current as the Bardeen polynomial that connects the covariant anomalies of the Fermi arcs and restores charge conservation, most notably when the Fermi surface knots into a bowtie. We expect that the bowtie Fermi surface and its response to external fields will be important to understand strained Weyl semimetals experimentally, in particular, their transport properties.

Our work highlights that measuring the consistent or covariant anomaly (e.g., the factor of 1/3) depends on whether the experimental probe is sensible to only the Fermi surface or rather the entire Fermi sea. Additionally, perturbations such as strain allow other model parameters to depend on position, e.g., the Fermi velocity, as well as additional terms in Eq. (7) [59]. Our work motivates the study of these questions to interpret incipient experiments in strained Weyl semimetals.

We thank B. Bradlyn, Y. Ferreiros, R. Ilan, F. de Juan, K. Landsteiner, and D. Pesin for insightful discussions, and especially N. G. Goldman for discussions that initiated this work and comments on the manuscript. This research was funded by the Marie Curie Program under EC Grant Agreement No. 653846 (A.G.G.), the ERC Starting Grant No. 679722, and the Knut and Alice Wallenberg Foundation 2013-0093 (J.H.B.), the EPSRC Grant No. EP/N01930X/1 (S.R.), and supported by the Laboratory Directed Research and Development (LDRD) funding from Lawrence Berkeley National Laboratory, provided by the Director, Office of Science, of the U.S. Department of Energy under Contract No. DEAC02-05CH11231, and the DOE Basic Energy Sciences (BES) TIMES initiative as well as UTD Research Enhancement Funds (M.H.K.).

[1] R. A. Bertlmann, *Anomalies in Quantum Field Theory*, International Series of Monographs in Physics Vol. 91 (Oxford University Press, Oxford, UK, 2000).

[2] S. L. Adler, Axial-vector vertex in spinor electrodynamics, Phys. Rev. **177**, 2426 (1969).

[3] J. S. Bell and R. Jackiw, A PCAC puzzle: $\pi^0 \to \gamma\gamma$ in the σ-model, Nuovo Cimento A **60**, 47 (1969).

[4] A. M. Turner and A. Vishwanath, Beyond band insulators: Topology of semimetals and interacting phases, in *Topological Insulators*, edited by M. Franz and L. Molenkamp, Contemporary Concepts of Condensed Matter Science Vol. 6 (Elsevier, Amsterdam, 2013), Chap. 11, pp. 293–324.

[5] P. Hosur and X. Qi, Recent developments in transport phenomena in Weyl semimetals, C. R. Phys. **14**, 857 (2013).

[6] V. A. Miransky and I. A. Shovkovy, Quantum field theory in a magnetic field: From quantum chromodynamics to graphene and Dirac semimetals, Phys. Rep. **576**, 1 (2015).

[7] S. Jia, S.-Y. Xu, and M. Z. Hasan, Weyl semimetals, Fermi arcs and chiral anomalies, Nat. Mater. **15**, 1140 (2016).

[8] A. A. Burkov, Topological semimetals, Nat. Mater. **15**, 1145 (2016).

[9] N. P. Armitage, E. J. Mele, and A. Vishwanath, Weyl and Dirac semimetals in three-dimensional solids, Rev. Mod. Phys. **90**, 015001 (2018).

[10] H. B. Nielsen and M. Ninomiya, The Adler-Bell-Jackiw anomaly and Weyl fermions in a crystal, Phys. Lett. B **130**, 389 (1983).

[11] B. R. Holstein, Anomalies for pedestrians, Am. J. Phys. **61**, 142 (1993).

[12] O. Parrikar, T. L. Hughes, and R. G. Leigh, Torsion, parity-odd response, and anomalies in topological states, Phys. Rev. D **90**, 105004 (2014).

[13] L. Sun and S. Wan, Chiral viscoelastic response in Weyl semimetals, Europhys. Lett. **108**, 37007 (2014).

[14] M. A. Zubkov, Emergent gravity and chiral anomaly in Dirac semimetals in the presence of dislocations, Ann. Phys. (NY) **360**, 655 (2015).

[15] A. Cortijo, Y. Ferreirós, K. Landsteiner, and M. A. H. Vozmediano, Elastic Gauge Fields in Weyl Semimetals, Phys. Rev. Lett. **115**, 177202 (2015).

[16] D. I. Pikulin, A. Chen, and M. Franz, Chiral Anomaly from Strain-Induced Gauge Fields in Dirac and Weyl Semimetals, Phys. Rev. X **6**, 041021 (2016).

[17] A. G. Grushin, J. W. F. Venderbos, A. Vishwanath, and R. Ilan, Inhomogeneous Weyl and Dirac Semimetals: Transport in Axial Magnetic Fields and Fermi Arc Surface States from Pseudo-Landau Levels, Phys. Rev. X **6**, 041046 (2016).

[18] Y. You, G. Y. Cho, and T. L. Hughes, Response properties of axion insulators and Weyl semimetals driven by screw dislocations and dynamical axion strings, Phys. Rev. B **94**, 085102 (2016).

[19] K. Landsteiner, E. Megías, and F. Pena-Benitez, Gravitational Anomaly and Transport Phenomena, Phys. Rev. Lett. **107**, 021601 (2011).

[20] J. Gooth, A. C. Niemann, T. Meng, A. G. Grushin, K. Landsteiner, B. Gotsmann, F. Menges, M. Schmidt, C. Shekhar, V. Süß, R. Hühne, B. Rellinghaus, C. Felser, B. Yan, and K. Nielsch, Experimental signatures of the mixed axial–gravitational anomaly in the Weyl semimetal NbP, Nature (London) **547**, 324 (2017).

[21] Y. Ferreiros, Y. Kedem, E. J. Bergholtz, and J. H. Bardarson, Mixed Axial-Torsional Anomaly in Weyl Semimetals, Phys. Rev. Lett. **122**, 056601 (2019).

[22] L. Lepori, M. Burrello, and E. Guadagnini, Axial anomaly in multi-Weyl and triple-point semimetals, J. High Energy Phys. 06 (2018) 110.

[23] T. D. C. Bevan, A. J. Manninen, J. B. Cook, J. R. Hook, H. E. Hall, T. Vachaspati, and G. E. Volovik, Momentum creation by vortices in superfluid ^{3}He as a model of primordial baryogenesis, Nature (London) **386**, 689 (1997).

[24] F. R. Klinkhamer and G. E. Volovik, Emergent *CPT* violation from the splitting of Fermi points, Int. J. Mod. Phys. A **20**, 2795 (2005).

[25] C.-X. Liu, P. Ye, and X.-L. Qi, Chiral gauge field and axial anomaly in a Weyl semimetal, Phys. Rev. B **87**, 235306 (2013).

[26] M. N. Chernodub, A. Cortijo, A. G. Grushin, K. Landsteiner, and M. A. H. Vozmediano, Condensed matter realization of the axial magnetic effect, Phys. Rev. B **89**, 081407(R) (2014).

[27] T. Schuster, T. Iadecola, C. Chamon, R. Jackiw, and S. Y. Pi, Dissipationless conductance in a topological coaxial cable, Phys. Rev. B **94**, 115110 (2016).

[28] Z.-M. Huang, J. Zhou, and S.-Q. Shen, Topological responses from chiral anomaly in multi-Weyl semimetals, Phys. Rev. B **96**, 085201 (2017).

[29] J.-H. Zhou, H. Jiang, Q. Niu, and J.-R. Shi, Topological invariants of metals and the related physical effects, Chin. Phys. Lett. **30**, 027101 (2013).

[30] H. Sumiyoshi and S. Fujimoto, Torsional Chiral Magnetic Effect in a Weyl Semimetal with a Topological Defect, Phys. Rev. Lett. **116**, 166601 (2016).

[31] A. Cortijo, D. Kharzeev, K. Landsteiner, and M. A. H. Vozmediano, Strain-induced chiral magnetic effect in Weyl semimetals, Phys. Rev. B **94**, 241405(R) (2016).

[32] A. Weststrom and T. Ojanen, Designer Curved-Space Geometry for Relativistic Fermions in Weyl Metamaterials, Phys. Rev. X **7**, 041026 (2017).

[33] E. V. Gorbar, V. A. Miransky, I. A. Shovkovy, and P. O. Sukhachov, Pseudomagnetic lens as a valley and chirality splitter in Dirac and Weyl materials, Phys. Rev. B **95**, 241114(R) (2017).

[34] E. V. Gorbar, V. A. Miransky, I. A. Shovkovy, and P. O. Sukhachov, Second-order chiral kinetic theory: Chiral magnetic and pseudomagnetic waves, Phys. Rev. B **95**, 205141 (2017).

[35] E. V. Gorbar, V. A. Miransky, I. A. Shovkovy, and P. O. Sukhachov, Pseudomagnetic helicons, Phys. Rev. B **95**, 115422 (2017).

[36] S. Roy, M. Kolodrubetz, N. Goldman, and A. G. Grushin, Tunable axial gauge fields in engineered Weyl semimetals: Semiclassical analysis and optical lattice implementations, 2D Mater. **5**, 024001 (2018).

[37] S. A. Yang, H. Pan, and F. Zhang, Chirality-Dependent Hall Effect in Weyl Semimetals, Phys. Rev. Lett. **115**, 156603 (2015).

[38] Q.-D. Jiang, H. Jiang, H. Liu, Q.-F. Sun, and X. C. Xie, Topological Imbert-Fedorov Shift in Weyl Semimetals, Phys. Rev. Lett. **115**, 156602 (2015).

[39] A. Cortijo and M. A. Zubkov, Emergent gravity in the cubic tight-binding model of Weyl semimetal in the presence of elastic deformations, Ann. Phys. (NY) **366**, 45 (2016).

[40] K. Landsteiner, Notes on anomaly induced transport, Acta Phys. Pol. B **47**, 2617 (2016).

[41] K. Landsteiner, Anomalous transport of Weyl fermions in Weyl semimetals, Phys. Rev. B **89**, 075124 (2014).

[42] E. V. Gorbar, V. A. Miransky, I. A. Shovkovy, and P. O. Sukhachov, Consistent Chiral Kinetic Theory in Weyl Materials: Chiral Magnetic Plasmons, Phys. Rev. Lett. **118**, 127601 (2017).

[43] W. A. Bardeen, Anomalous ward identities in spinor field theories, Phys. Rev. **184**, 1848 (1969).

[44] E. V. Gorbar, V. A. Miransky, I. A. Shovkovy, and P. O. Sukhachov, Origin of Bardeen-Zumino current in lattice models of Weyl semimetals, Phys. Rev. B **96**, 085130 (2017).

[45] E. V. Gorbar, V. A. Miransky, I. A. Shovkovy, and P. O. Sukhachov, Chiral magnetic plasmons in anomalous relativistic matter, Phys. Rev. B **95**, 115202 (2017).

[46] M. M. Vazifeh and M. Franz, Electromagnetic Response of Weyl Semimetals, Phys. Rev. Lett. **111**, 027201 (2013).

[47] A. G. Grushin, J. W. F. Venderbos, and J. H. Bardarson, Coexistence of Fermi arcs with two-dimensional gapless Dirac states, Phys. Rev. B **91**, 121109(R) (2015).

[48] Z. Wang, Y. Sun, X.-Q. Chen, C. Franchini, G. Xu, H. Weng, X. Dai, and Z. Fang, Dirac semimetal and topological phase transitions in A_3Bi (A = Na, K, Rb), Phys. Rev. B **85**, 195320 (2012).

[49] Z. Wang, H. Weng, Q. Wu, X. Dai, and Z. Fang, Three-dimensional Dirac semimetal and quantum transport in Cd_3As_2, Phys. Rev. B **88**, 125427 (2013).

[50] H. Weng, C. Fang, Z. Fang, B. A. Bernevig, and X. Dai, Weyl Semimetal Phase in Noncentrosymmetric Transition-Metal Monophosphides, Phys. Rev. X **5**, 011029 (2015).

[51] See Supplemental Material at http://link.aps.org/supplemental/10.1103/PhysRevB.99.140201 for a brief summary of the consistent and covariant anomalies, a detailed description of the numerical implementation of the response functions, and a discussion of the finite size and mass corrections, which includes Refs. [60–66].

[52] We restrict our analysis to isotropic Weyl nodes for simplicity.

[53] H. J. Rothe, *Lattice Gauge Theories: An Introduction* (World Scientific, Singapore, 2005).

[54] The Fermi surface rectangle becomes a parallelogram for general orientations of **B**.

[55] D. Bulmash and X.-L. Qi, Quantum oscillations in Weyl and Dirac semimetal ultrathin films, Phys. Rev. B **93**, 081103(R) (2016).

[56] Y. Ominato and M. Koshino, Magnetotransport in Weyl semimetals in the quantum limit: Role of topological surface states, Phys. Rev. B **93**, 245304 (2016).

[57] N. Bovenzi, M. Breitkreiz, T. E. OBrien, J. Tworzydlo, and C. W. J. Beenakker, Twisted Fermi surface of a thin-film Weyl semimetal, New J. Phys. **20**, 023023 (2018).

[58] Such bulk to surface charge transfer is a property of clean systems where the scattering time $\tau \to \infty$. For a finite amount of disorder, the charge buildup will be screened faster than it diffuses, but this regime is outside of the scope of this work.

[59] V. Arjona and M. A. H. Vozmediano, Rotational strain in Weyl semimetals: A continuum approach, Phys. Rev. B **97**, 201404(R) (2018).

[60] K. G. Wilson, Confinement of quarks, Phys. Rev. D **10**, 2445 (1974).

[61] R. Jackiw and A. Kostelecky, Radiatively Induced Lorentz and *CPT* Violation in Electrodynamics, Phys. Rev. Lett. **82**, 3572 (1999).

[62] M. Pérez-Victoria, Exact Calculation of the Radiatively Induced Lorentz and *CPT* Violation in QED, Phys. Rev. Lett. **83**, 2518 (1999).

[63] M. Stone, Gravitational anomalies and thermal Hall effect in topological insulators, Phys. Rev. B **85**, 184503 (2012).

[64] S. Roy, M. Kolodrubetz, J. E. Moore, and A. G. Grushin, Chern numbers and chiral anomalies in Weyl butterflies, Phys. Rev. B **94**, 161107(R) (2016).

[65] S. Chandrasekharan, Anomaly cancellation in 2+1 dimensions in the presence of a domain wall mass, Phys. Rev. D **49**, 1980 (1994).

[66] A. G. Grushin, Consequences of a condensed matter realization of Lorentz-violating QED in Weyl semi-metals, Phys. Rev. D **86**, 045001 (2012).